The Cryosphere Discuss., 6, 793–819, 2012
www.the-cryosphere-discuss.net/6/793/2012/
doi:10.5194/tcd-6-793-2012


The Cryosphere Discussions



# P-wave velocity changes in freezing hard low-porosity rocks: a laboratory-based time-average model

**D. Draebing and M. Krautblatter**

Department of Geography, Bonn, Germany

Received: 26 January 2012 – Accepted: 6 February 2012 – Published: 21 February 2012

Correspondence to: D. Draebing (daniel.draebing@giub.uni-bonn.de)

Published by Copernicus Publications on behalf of the European Geosciences Union.







## Abstract

P-wave refraction seismics is a key method in permafrost research but its applicability to low-porosity rocks, that constitute alpine rock walls, has been denied in prior studies. These explain p-wave velocity changes in freezing rocks exclusively due to changing velocities of pore infill, i.e. water, air and ice. In existing models, no velocity increase is expected for low-porosity bedrock. We postulate, that mixing laws apply for high-porosity rocks, but freezing in confined space in low-porosity bedrock also alters physical rock matrix properties. In the laboratory, we measured p-wave velocities of 22 decimeter-large low-porosity (<6 %) metamorphic, magmatic and sedimentary permafrost rock samples with a natural texture (>100 micro-fissures) from 25 °C to –15 °C in 0.3 °C increments close to the freezing point. P-wave velocity increases by 7–78 % when freezing parallel to cleavage/bedding and matrix velocity increases from 5–59 % coincident to an anisotropy decrease in most samples. The expansion of rigid bedrock upon freezing is restricted and ice pressure will increase matrix velocity and decrease anisotropy while changing velocities of the pore infill are insignificant. Here, we present a modified Timur's 2-phase equation implementing changes in matrix velocity dependent on lithology and demonstrate the physical basis for refraction seismics in low-porosity bedrock.

## 1 Introduction

Most polar and many mountainous regions of the earth are underlain by permafrost and are susceptible to Climate Change (IPCC, 2007; Nogués-Bravo et al., 2007). Permafrost is a thermally defined phenomenon referring to ground that remains below 0 °C for at least two consecutive years (NRC-Permafrost-Subcommitee, 1988). Rock permafrost is not synonymous with perennially frozen rock due to freezing point depression resulting from solutes, pressure, pore diameter and pore material (Lock, 2005; Krautblatter et al., 2010). Ice develops in pores and cavities (Hallet et al., 1991) and





TCD
6, 793–819, 2012



affects the thermal, hydraulic and mechanical properties of rocks. Climate Change acts to degrade permafrost and, thus, alters permafrost distribution. In mountainous regions, degrading permafrost rock walls are considered to be a major hazard due to rockfall activity and slow rock deformation (Gruber and Haeberli, 2007; Krautblatter et al., 2012).

Surface-based geophysical methods represent a cost-effective approach for permafrost characterization (Harris et al., 2001). The application of geophysical methods has a long tradition in permafrost studies (Barnes, 1966; Akimov et al., 1973; Ferrians and Hobson, 1973; Scott et al., 1979, 1990). Hauck and Kneisel (2008) and Kneisel et al. (2008) provide an overview about geophysical methods suitable for permafrost monitoring in high-mountain environments. In contrast to direct temperature measurements in boreholes, geophysical methods provide only indirect information about permafrost occurrence. On the other hand, geophysical methods are non-invasive, provide spatial 2-D/3-D information and are also applicable in instable fractured rock. Frozen ground changes the properties of underground materials, the degree of change depends on water content, pore size, pore water chemistry, underground temperature and material pressure (Scott et al., 1979, 1990). The most prominent geophysical parameters for the differentiation between frozen and unfrozen underground are electrical resistivity and compressional wave velocity (Hauck, 2001). Alpine rock cliffs in permafrost regions mostly consist of hard low-porosity (<5 %) rocks and it is yet unclear to what extend geophysical methods can be applied to them. While the relationship between electrical resistivity and frozen low-porosity bedrock has been investigated by Krautblatter et al. (2010), this article will focus on the applicability of p-wave refraction seismics to such rocks.

P-wave velocity of freezing rocks was investigated in the laboratory mostly using polar high-porosity sedimentary rocks (Timur, 1968; Dzhurik and Leshchikov, 1973; King, 1977; Pandit and King, 1979; Pearson et al., 1986; Remy et al., 1994; Sondergeld and Rai, 2007; Bonner et al., 2009). Low-porosity igneous rocks were studied by Takeuchi and Simmons (1973) and Toksöz et al. (1976). Early laboratory studies demonstrated





TCD
6, 793–819, 2012



compressional and shear wave velocity increases in freezing bedrock (Timur, 1968; King, 1977). Seismic velocities increase at sub-zero temperatures until they reach a plateau when most of the pores are frozen and the unfrozen water content is negligible (Pandit and King, 1979; Pearson et al., 1986). P-wave velocity of freezing rocks is controlled by the original water-filled porosity, i.e. the velocity corresponds to the changing proportion of frozen and unfrozen pore water content (King et al., 1988). In that sense, saline pore water increases the unfrozen pore water content at a given temperature (Anderson and Morgenstern, 1973; Tice et al., 1978) and flattens the otherwise sharp p-wave velocity increase when freezing (Pandit and King, 1979). Some authors observed hysteresis effects between ascending and descending temperature runs and assumed supercooling of the pore water on the descending temperature run as a reason (Nakano et al., 1972; King, 1977).

These findings have been transferred to field applications of p-wave velocity refraction seismics to various sedimentary landforms in polar (Roethlisberger, 1961; Kurfurst and Hunter, 1977; King, 1984; Harris and Cook, 1986; Zimmerman and King, 1986; Bonner et al., 2009) and to rock glaciers (Barsch, 1973; Musil et al., 2002; Ikeda, 2006; Hausmann et al., 2007), to bedrock (Hauck et al., 2004) and to talus slopes (Hilbich, 2010) in mountainous regions. Akimov et al. (1973) note a discrepancy between seismic results in the laboratory and in the field. They further assume a high rate of cooling, a non-representation of the stressed state of earth, supercooling and the time required for transition into ice. This article will provide some answers with respect to these shortcomings.

Carcione and Seriani (1998) give an overview about existing modelling of permafrost based on seismic velocities mostly for unconsolidated porous media (Zimmerman and King, 1986; King et al., 1988; Leclaire et al., 1994). Wyllie et al. (1956) developed a time-average equation

$$\frac{1}{v} = \frac{\Phi}{v_{\mathrm{l}}} + \frac{1-\Phi}{v_{\mathrm{m}}}, \tag{1}$$





TCD
6, 793–819, 2012



where $v$ is the velocity measured, $v_l$ is the velocity in saturating liquid, $v_m$ is the matrix velocity and $\Phi$ is the volumetric porosity fraction, based on measurements of sandstone ($0.02 < \Phi < 0.32$) and limestone samples ($0.001 < \Phi < 0.18$). Later, Wyllie et al. (1958) excluded carbonates from their equation due to the independent behaviour of p-wave velocities of porosities. The two-phase model of Timur (1968) modified the Eq. (1) to frozen states,

$$\frac{1}{v} = \frac{\Phi}{v_i} + \frac{1-\Phi}{v_m} \tag{2}$$

where $v_i$ is the velocity of ice in the pore space. Timur (1968) extended Eq. (2) to a three-phase time-average equation:

$$\frac{1}{v} = \frac{(1-S_i)\Phi}{v_l} + \frac{S_i\Phi}{v_i} + \frac{1-\Phi}{v_m} \tag{3}$$

with $S_i$ is the relative fraction of pore space occupied by ice. Equations (2 and 3) were tested for sandstone ($0.13 < \Phi < 0.42$), carbonate ($0.15 < \Phi < 0.17$) and shale samples ($0.04 < \Phi < 0.10$). McGinnis et al. (1973) deduced that the relative p-wave velocity increases upon freezing $\Delta v_p$ (%) versus porosity is

$$\Delta v_p = \frac{\Phi - 0.0363}{0.0044} \tag{4}$$

based on a linear regression of Timur's (1968) measurements. This relation postulates that there is no p-wave velocity acceleration due to freezing in rocks with porosities less than 3.63 % and hardly any in low-porosity rocks (<5 %). Hauck et al. (2011) extended Timur's (1968) equation to 4 phases and weighted the p-wave velocities of the components by their volumetric fractions:

$$\frac{1}{v} = \frac{f_l}{v_l} + \frac{f_m}{v_m} + \frac{f_i}{v_i} + \frac{f_a}{v_a} \tag{5}$$

$$f_l + f_m + f_i + f_a = 1 \text{ and } 0 \le f_l, f_m, f_i, f_a \le 1 \tag{6}$$





TCD
6, 793–819, 2012



where $v_a$ is the velocity of air, $f_l$ is the volumetric fraction for liquid water, $f_r$ is the volumetric fraction for rock, $f_i$ is the volumetric fraction for ice and $f_a$ is the volumetric fraction for air.

The influence of pressure on seismic velocities is observed by many researchers (King, 1966; Nur and Simmons, 1969; Takeuchi and Simmons, 1973; Toksöz et al., 1976; Wang, 2001). Two pressures can be distinguished, the confining or overburden pressure of the rock mass and the pore pressure of the fluid. The effective pressure ($P_e$) is

$$P_e = P_c - nP_p, \tag{7}$$

where $P_c$ is the confining pressure, $P_p$ is the pore pressure and $n \leq 1$. The net overburden pressure ($P_d$) is then described as

$$P_d = P_c - P_p. \tag{8}$$

Confining pressure and saturation-triggered pore pressure can reinforce or compete with each other which can be expressed by different values of $n$ (Wang, 2001) and results in changes of seismic velocities (Nur and Simmons, 1969) and porosity (Takeuchi and Simmons, 1973; Toksöz et al., 1976). Pores react to increasing pressure according to their shape: spheroidal pores deform and become thinner while spherical pores decrease in volume (Takeuchi and Simmons, 1973; Toksöz et al., 1976). The effect of pores is negligible with high confining pressures but the effects of cracks are large (Takeuchi and Simmons, 1973). For Permafrost conditions the ice pressure effect is most pronounced for spheroidal "flat" pores or cracks (Toksöz et al., 1976).

Pore shape, cracks and fractures also determine seismic anisotropy next to anisotropic mineral components and textural-structural characteristics as bedding and cleavage (Lo et al., 1986; Thomsen, 1986; Vernik and Nur, 1992; Wang, 2001; Barton, 2007). The two latter causes are referred to as intrinsic anisotropy and cannot decrease as a result of pressure (Lo et al., 1986; Thomsen, 1986; Barton, 2007). In contrast, "induced anisotropy" through pores, cracks and fractures corresponds to stress. Thus,





TCD
6, 793–819, 2012



seismically isotropic rocks can become more anisotropic (Wang, 2001; Barton, 2007) and vice versa due to pressure alteration. Anisotropy $A$ is defined as

$$A = \frac{v_{max} - v_{min}}{v_{max}}, \quad (9)$$

where $v$ is the velocity of compressional waves parallel and perpendicular to cleavage or bedding (Johnston and Christensen, 1995).

We postulate that p-wave velocity measurements in low-porosity rocks could become an important method for the monitoring of Alpine rock wall permafrost. This study tries to overcome the discrepancy between laboratory and field p-wave refraction seismics as mentioned by Akimov et al. (1973). The study aims at (1) measuring the p-wave velocity increases in low-porosity rocks, (2) evaluating the increase of matrix velocity due to ice pressure, (3) describing the alteration of seismic anisotropy due to changes of induced pore pressure and (4) incorporating this matrix velocity increase in the time-average equation.

## 2 Methodology

We tested 22 rock specimens between 1.8 and 25 kg sampled from several Alpine and Arctic permafrost sites. We used large rock specimen with a statistical distribution of $>10^2$ of fissures, cracks and cleavages to cope with their natural heterogeneity (Akimov et al., 1973; Matsuoka and Murton, 2008; Jaeger, 2009). All samples were immersed in water under atmospheric conditions for at least 48 h to a constant weight. Pore space was fully saturated under atmospheric pressure, as free saturation resembles the field situation more closely than saturation under vacuum conditions (Krus, 1995; Sass, 2005). After that the samples are dried at 105 °C to a constant weight. The water absorption capacity $W_A$ is

$$W_A = \frac{(W_s - W_d)}{W_d} * 100 \quad (10)$$





TCD
6, 793–819, 2012



where $W_s$ is the weight of the sample after at least 48 h water saturation to a constant weight and $W_d$ is the weight of the sample dried at 105 °C to a constant weight. Rock density $\rho$ is derived from Wohlenberg (2012). The effective porosity $\Phi_{eff}$

$$\Phi_{eff} = W_A * \rho \tag{11}$$

is calculated by multiplying the water absorption capacity with the rock density and includes only hydraulical-linked pores (Sass, 2005). Using the samples presented in this paper, six plan-parallel cylindrical plugs were prepared with diameter and length of 30 mm and porosity values were measured using a gas compression/expansion method in a Micromeritics Multivolume Pycnomter 1305 by Krautblatter (2009). These porosity values are used to estimate the quality of the effective porosity values. All samples were immersed for 48 h under atmospheric conditions and the saturated weight $W_{48\ h}$ were determined. To determine the moisture conditions we calculated the degree of saturation $S_r$

$$S_r = \frac{(W_{48\ h} - W_d)}{(W_s - W_d)}. \tag{12}$$

Subsequently, samples were loosely coated with plastic film to protect them against drying and were cooled in a range of 25 °C to –15 °C in a WEISS WK 180/40 high-accuracy climate chamber. The cooling rate was first 7 °C $h^{-1}$ until 0 °C and was then decreased to 6 °C $h^{-1}$ (Matsuoka, 1990). Ventilation was applied to avoid thermal layering. Two to three calibrated 0.03 °C-accuracy thermometers measured rock temperature at different depths to account for temperature homogeneity in the sample (Krautblatter et al., 2010). The p-wave generator and the receiver were placed on flattened or cut opposite sides of the cuboid samples. The traveltime of the p-wave was picked using a Fluke Scopemeter with an accuracy of 1–2 × $10^{-6}$ s. The internal deviation induced by the measurement procedure was assessed by conducting five subsequent traveltime measurements. To account for the anisotropy of the rock samples, we measured p-wave velocities in the same sample in the direction of cleavage/bedding and





TCD
6, 793–819, 2012



perpendicular to the cleavage/bedding direction. The matrix velocity $v_m$ is calculated by solving Eq. (2). The velocity of the material in the pore space $v_i$ is 1570 m s$^{-1}$ for water in the unfrozen status and 3310 m s$^{-1}$ for ice (Timur, 1968). Matrix velocity is calculated for frozen and unfrozen status both for parallel and perpendicular to cleavage/bedding measurements according to

$$V_m = \frac{(1-\Phi)}{\left(\frac{1}{v} - \frac{\Phi}{v_i}\right)} \quad (13)$$

The change of matrix velocity $\Delta V_m$ due to freezing is calculated according to

$$\Delta V_m = \frac{(V_{mf} - V_{ms})}{V_{ms}} \quad (14)$$

where $V_{mf}$ is the matrix velocity in the frozen status and $V_{ms}$ is the matrix velocity in the saturated status. The change of Anisotropy $\Delta A$ due to freezing will be calculated according to:

$$\Delta A = A_s - A_f \quad (15)$$

where $A_s$ is the anisotropy after 48 h saturation and $A_f$ is the anisotropy for frozen status.

## 3 Results

Table 1 gives an overview about measured rock samples and their rock properties and seismic velocities. Figure 1 represents the evolution of p-wave velocities dependent on rock temperature of six selected rock samples from six different lithologies.





TCD
6, 793–819, 2012



### 3.1 Porosities and degree of saturation

The absolute (vacuum) porosity values measured for 6 samples (A5, X2, S1, S3, X9, A8) by Krautblatter (2009) are compared with the effective (atmospheric pressure) porosity values. The absolute porosity ($2.60 \pm 0.21$ %) is on average 30 % higher than the effective porosity ($1.72 \pm 0.12$ %), only in slate samples both were equivalent.

Rock samples are classified according to their lithology into three metamorphic, two igneous and two sedimentary rock clusters. All clusters differ less than 1 % in effective porosity except carbonates. After 48 h saturation, gneiss, plutonic rocks, volcanic rocks and clastic rocks show mean $S_r$ of 1.00, other metamorphic rocks (mean $S_r = 0.98$), schists (mean $S_r = 0.97$) and carbonate rocks (mean $S_r = 0.98$) are not fully saturated but all are subject to develop cryostatic pressure upon the volumetric expansion of ice in more than 91 % saturated pores (Walder and Hallet, 1986).

### 3.2 P-wave velocities of frozen rock

In contrast to Eq. (4), p-wave velocity increases significantly as a result of freezing in all 22 samples. Parallel to cleavage/bedding, p-wave velocity increase is highest in sedimentary (carbonate and clastic) rocks, followed by magmatic (volcanic and plutonic) rocks and lowest in metamorphic rocks (schists, other metamorphic rocks and gneiss) (Fig. 2a). The order remains the same perpendicular to cleavage/bedding except for schists (Fig. 2b).

### 3.3 Porosity dependent change in p-wave velocities

Existing time-average models assume a dependence of p-wave velocity increase from porosity. We plotted the increase of p-wave velocity due to freezing against the mean effective porosity (Fig. 3). Metamorphic and igneous rocks show only a negligible scattering for parallel measurements. The p-wave velocities of clastic rocks with comparable porosities increase between 13 and 50 % due to freezing. Carbonate rocks show





TCD
6, 793–819, 2012



similar p-wave velocity increase (78 ± 7 %) in spite of highly scattered porosity values (24 ± 22 %). Perpendicular to cleavage or bedding, igneous and metamorphic rocks except the schists show negligible scattering. Values for schists differ from 10 % to 165 % increase for comparable effective porosities, values for clastic rocks scatter between 13 and 38 %. Low porous dolomite shows a p-wave velocity increase of 223 % due to freezing while p-wave velocities of high porous limestone rise by 109 %. Supercooling causes hysteresis effects in 16 of 22 samples.

### 3.4 Matrix velocity

The increase in p-wave velocity is too high to be explained by changes of the p-wave velocity in the pore infill as is suggested by Timur (1968) and McGinnis et al. (1973). Here, the additional change in p-wave velocity is explained by the increase in matrix velocity as shown in Eqs. (13) and 14). All measured rock samples show a significant matrix velocity increases $v_m$ due to freezing except the sample X5. Figure 4a and b show that bulk p-wave velocity changes when freezing closely correlate to changes in calculated matrix velocities while changes in pore infill are insignificant.

### 3.5 Anisotropy

Anisotropy $A$ is calculated according to Eq. (9) for conditions after 48 h saturation ($A_s$) and frozen conditions at –15 °C ($A_f$). Induced anisotropy due to pores, cracks and fractures can be reduced through pressure (Wang, 2001; Barton, 2007). Anisotropy alteration $\Delta A$ is calculated according to Eq. (15). In our experimental setup, pore ice pressure reduces induced anisotropy due to the closure of pores, cracks and fractures, while the confining (atmospheric) pressure remains constant. The pore pressure changes due to the phase transition from water to ice in saturated pores. Ice develops pressure through volumetric expansion and ice segregation (Matsuoka, 1990; Matsuoka and Murton, 2008). Frost weathering represents a result of ice pressure (Matsuoka, 1990; Vlahou and Worster, 2010). 15 of 22 samples show an anisotropy





TCD
6, 793–819, 2012



reduction due to freezing (1–45 %), which is especially pronounced in slates, schists and carbonates. Seven samples show negligible ($n = 3$, $< 1.50$ %) or small ($n = 4$, $\leq 3.50$ %) increases in anisotropy when freezing. Three samples (L1, L2, M1) show a low anisotropy increase, the anisotropy of four other samples (H1, H2, X2, X7) increases slightly.

## 4 Discussion

### 4.1 Model setup and representativity

This study aims at overcoming the discrepancies between field and laboratory measurements in high mountain areas with hard low-porosity rocks. Previous studies (Timur, 1968; McGinnis et al., 1973) explained p-wave velocity increases exclusively as an effect of porosity and infill. We postulate, that these models apply well for soft high-porosity rocks but cannot be transferred to hard low-porosity rocks. This is due to the fact that the effects of freezing are determined by multiple effects including (i) porosity but also (ii) the pore form and the degree of fissuring, (iii) ice pressure development. Here, we try to derive a straightforward model that explains the effects of freezing in low-porosity rocks on p-wave velocity.

(i) We have tested 6 clusters or 20 specimen (except carbonates, see Wyllie et al. (1958)) of low-porosity rocks. These indicate p-wave velocity increases from $7.3 \pm 3.7$ % (gneiss), $15.8 \pm 4.4$ % (other metamorphic rocks), $16.7 \pm 7.9$ % (schists), $17.7 \pm 0.6$ % (plutonic rocks), $31.6 \pm 6.5$ % (volcanic rocks) to $31.4 \pm 18.5$ % (clastic rocks). The McGinnis et al. (1973) model would respectively anticipate changes from 0 % (gneiss), 0 % (other metamorphic rocks), 0 % (schists), 0 % (plutonic rocks), 0 % (volcanic rocks) to 4.5 % (clastic rocks) and is incapable of explaining p-wave velocity increases in low-porosity bedrock (Fig. 3b). This shows that porosity is not the relevant determinant of p-wave velocity changes in low-porosity bedrock.





TCD
6, 793–819, 2012



(ii) Pore form is among the most important factors for seismic properties (Nur and Simmons, 1969; Toksöz et al., 1976; Wang, 2001) and the most difficult one to quantify (Wang, 2001). Pore form determines pressure susceptibility (Takeuchi and Simmons, 1973; Toksöz et al., 1976) and ice effects (Toksöz et al., 1976) while pore linkage affects the saturation. Water-saturated porosity controls p-wave velocity (King, 1977; King et al., 1988) and frost weathering (Matsuoka, 1990; Sass, 2005; Matsuoka and Murton, 2008). We assume no influence of salinity due to low solubility of rock minerals in the used specimens (Krautblatter, 2009). Hydraulically linked porosity is best described by effective porosity (Sass, 2005) and we replace porosity in Eq. (2) with effective porosity. However, the resulting matrix velocity would change only by $2 \pm 2\,\%$ when assuming absolute or effective porosity for non-carbonates and carbonates should generally be excluded due to internal solution processes (Wyllie et al., 1958). The weathering history determines the development of pores, fissures and fractures in permafrost and non-permafrost samples. We choose decimeter-large rock samples from Alpine and Arctic permafrost sites instead of standard bore cores. These include hundreds of micro-fissures and statistically better represent the natural texture of permafrost-affected bedrock. This reflects, that properties like pore distribution, texture, fissures and fractures provide the space and determine the effects of confined ice growth in hard rock samples (Matsuoka and Murton, 2008). Previous studies mostly used high-porosity arctic specimens from Mesozoic sedimentary rocks (Timur, 1968; McGinnis et al., 1973; King, 1977; Pandit and King, 1979; Pearson et al., 1986; Sondergeld and Rai, 2007; Bonner et al., 2009) and frost susceptibility in these low-strength rocks operates at a millimeter- to centimeter-scale (Matsuoka and Murton, 2008). In hard rocks, volumetric expansion and ice segregation is restricted by the rigid matrix and ice growth in pores and fissures causes high levels of stress inside the samples.





TCD
6, 793–819, 2012



(iii) The alteration of confining pressure related to rock overburden is a long-lasting process on a millennium scale; while pore pressure changes steadily (Matsuoka and Murton, 2008). Frequent daily freeze-thaw-cycles reach a depth of approximately 30 cm (Matsuoka and Murton, 2008) while annual cycles often reach up to 5 m and more (Matsuoka et al., 1998). In our experiment the change in matrix velocity in combination with reduced anisotropy points towards "induced anisotropy" (Wang, 2001) in pores that reflects intrinsic stress generation. This can be generated by the ice pressure building (Matsuoka, 1990; Vlahou and Worster, 2010) due to volumetric expansion of in situ water (Hall et al., 2002; Matsuoka and Murton, 2008) and ice segregation (Walder and Hallet, 1985; Hallet, 2006; Murton et al., 2006). In the laboratory any open system allows water migration and enables ice segregation while closed systems with water saturated samples favor volumetric expansion (Matsuoka, 1990). Our experimental setup is a quasi-closed system; water is only in situ available due to saturation and ice can leave through pores and joints. Due to 48 h saturation, the degree of saturation reaches at least 0.91, the threshold for volumetric expansion (Walder and Hallet, 1986), in all samples. According to Sass (2005) and Matsuoka (1990) our quasi-closed system and fully saturated samples could be a good analogue to natural conditions.

Cooling rates of 6 °C $h^{-1}$ have been used by Matsuoka (1990) before and produce high expansion and freezing strain. Sass (2005) assumes high saturation of alpine rocks below the upper 10 cm. This is due to the fact that ice pressure is relaxed through ice deformation and ice expansion into free spaces (Tharp, 1987), ice extrusion (Davidson and Nye, 1985) and samples were observed contract in the long-term due to ice creep (Matsuoka, 1990). In our system, samples cool from all outer faces which presumably act to seal the sample with ice. On the other hand ice segregation along temperature gradients in fissured natural bedrock will cause suction up to several MPa (Walder and Hallet, 1985; Murton et al., 2006) and ice growth and presumably cause a persistent elevated level of cryostatic stress similar to our laboratory setup.





TCD
6, 793–819, 2012



### 4.2 A time-average model for low-porosity rock

Based on these results we modify Eq. (2) and extend the equation with the pressure-induced variable *m*. Lithology is a proxy for pore form in our model and we assume an elevated level of stress in cryostatic systems.

$$\frac{1}{v} = \frac{\Phi}{v_{\mathrm{i}}} + \frac{1-\Phi}{v_{\mathrm{m}}} * \frac{1}{\mathrm{m}} \tag{16}$$

where

$$m = 1 + \Delta V_{\mathrm{m}}; \tag{17}$$

$\Delta V_{\mathrm{m}}$ is the increase of matrix velocity empirically derived from our measurements and we use lithology as a proxy. We propose values of *m* of $1.05 \pm 0.04$ for gneiss, $1.14 \pm 0.04$ for other metamorphic rocks, $1.14 \pm 0.08$ for schists, $1.14 \pm 0.01$ for plutonic rocks, $1.26 \pm 0.06$ for volcanic rocks, $1.24 \pm 0.21$ for clastic rocks and $1.59 \pm 0.10$ for carbonate rocks or, alternatively a general *m* of $1.15 \pm 0.09$ excluding carbonate rocks (Table 1). The use of Eq. (16) enhances to differentiate between frozen and unfrozen status of low-porosity rocks and can facilitate interpretation of field data.

## 5 Conclusions

Here, we propose to incorporate the physical concept of freezing in confined space into geophysical modelling of p-wave velocities and present data (1) of p-wave measurements of 22 different alpine rocks, (2) evaluate the influence of ice pressure on seismic velocities, (3) determine anisotropic decrease due to ice pressure and (4) extend Timur's (1968) 2-phase model for alpine rocks:

1. All rock samples show a p-wave velocity increase dependent on lithology due to freezing. P-wave velocity increases from $7.3 \pm 3.7$ % for gneiss to $78.5 \pm 7.0$ % for carbonate rocks parallel to cleavage/bedding; perpendicular measurements show





TCD
6, 793–819, 2012



an acceleration ranging from 11.1 ± 2.4 % for gneiss to 166.0 ± 56.9 % for carbonate rocks. The increase of p-wave velocity of carbonate rocks is independent of effective porosity, as has been outlined before by Wyllie et al. (1958). Especially schistosity strongly influences p-wave velocity increase perpendicular to cleavage due to freezing.

2. P-wave velocity increases due to freezing are dominated by an increase of the velocity of the rock matrix while changes in pore-infill velocities are insignificant. Matrix velocity increases parallel to cleavage/bedding from 5.08 ± 4.08 % for gneiss to 59.44 ± 9.93 % for carbonate rocks; perpendicular measurements indicate matrix velocity increase reaching from 8.95 ± 4.51 % for metamorphic rock group consisting of serpentine and amphibolite and 168.53 ± 62.00 % for carbonate rocks.

3. Anisotropy decreases by up to 45 % as a result of crack closure due to ice pressure in 15 of 22 rock samples.

4. We extend Timur's (1968) 2-phase equation with a lithology dependent variable to increase the Matrix velocity responding to developing ice pressure while freezing.

This study provides the physical basis for the applicability of refraction seismics in low-porosity permafrost rocks. Due to their rigidity low-porosity bedrock cannot expand freely in response to ice pressure and, thus, matrix velocity increases. P-wave velocity increases predominantly as a result of ice pressure and to a lesser extend as a result of the higher velocity of ice than water in pores. The extension of the time-average equation provides a more realistic calculation of the rock velocity and facilitates the interpretation of field data and possible permafrost distribution in alpine rock walls.

*Acknowledgements.* The authors thank G. Nover, J. Ritter and W. Scherer for equipment support to enable this study. Thanks to D. Funk for critical discussions, S. Verleysdonk for measurements, C. Hauck, C. Hilbich, L. Ravanel, A. Hasler, M. Siewert, P. Deline and M. Geilhausen for providing samples and all other involved persons.





## References


Akimov, A. T., Dostovalov, B. N., and Yakupov, V. S.: Geophysical methods of studying permafrost, 2nd International Conference on Permafrost, USSR Contribution, Yakutsk, USSR, 767–777, 1973.

Anderson, D. M., and Morgenstern, N. R.: Physics, chemistry, and mechanics of frozen ground: A review., 2nd International Conference on Permafrost. Northamerican Contribution, Yakutsk, USSR, 257–288, 1973.

Barnes, D. F.: Geophysical methods for delineating permafrost, 1st International Conference on Permafrost, LaFayette, Indiana 1963, 349–355, 1966,

Barsch, D.: Refraktionsseismische Bestimmung der Obergrenze des gefrorenen Schuttkörpers in verschiedenen Blockgletschern Graubündens, Schweizer Alpen, Zeitschrift für Gletscherkunde und Glazialgeologie, 9, 143–167, 1973.

Barton, N.: Rock quality, seismic velocity, attenuation and anisotropy, Routledge, London, Leiden, New York, 756 pp., 2007.

Bonner, J. L., Leidig, M. R., Sammis, C., and Martin, R. J.: Explosion Coupling in Frozen and Unfrozen Rock: Experimental Data Collection and Analysis, B. Seismol. Soc. Am., 99, 830–851, 2009.

Carcione, J. M. and Seriani, G.: Seismic and ultrasonic velocities in permafrost, Geophys. Prospec., 46, 441–454, doi:10.1046/j.1365-2478.1998.1000333.x, 1998.

Davidson, G. P. and Nye, J. F.: A Photoelastic Study of Ice Pressure in Rock Cracks, Cold Reg. Sci. Technol., 11, 141–153, 1985.

Dzhurik, V. and Leshchikov, F. N.: Experimental investigations of seismic properties of frozen soils, 2nd International Conference on Permafrost, USSR Contribution, Yakutsk, USSR, 485–488, 1973.

Ferrians, O. J. and Hobson, G. D.: Mapping and predicting permafrost in North America: A review, 1963–1973, 2nd International Conference on Permafrost. Northamerican Contribution, Yakutsk, USSR, 479–498, 1973.

Gruber, S. and Haeberli, W.: Permafrost in steep bedrock slopes and its temperature-related destabilization following climate change, J. Geophys. Res., 112, F02S18, doi:10.1029/2006JF000547, 2007.






TCD
6, 793–819, 2012



Hall, K., Thorn, C. E., Matsuoka, N., and Prick, A.: Weathering in cold regions: some thoughts and perspectives, Prog. Phys. Geog., 26, 577–603, 2002.
Hallet, B., Walder, J. S., and Stubbs, C. W.: Weathering by segregation ice growth in microcracks at sustained sub-zero temperatures: verification from an experimental study using acoustic emissions, Permafrost Periglac., 2, 283–300, doi:10.1002/ppp.3430020404, 1991.
Hallet, B.: Geology – Why do freezing rocks break?, Science, 314, 1092–1093, 2006.
Harris, C. and Cook, J. D.: The detection of high altitude permafrost in Jotunheimen, Norway using seismic refraction rechniques: an assessment, Arctic Alpine Res., 18, 19–26, 1986.
Harris, C., Davies, M. C. R., and Etzelmüller, B.: The assessment of potential geotechnical hazards associated with mountain permafrost in a warming global climate, Permafrost Periglac., 12, 145–156, 2001.
Hauck, C.: Geophysical methods for detecting permafrost in high mountains, 171, ETH Zurich, Zurich, 1–204, 2001.
Hauck, C., Isaksen, K., Vonder Mühll, D., and Sollid, J. L.: Geophysical surveys designed to delineate the altitudinal limit of mountain permafrost: an example from Jotunheimen, Norway, Permafrost Periglac., 15, 191–205, 2004.
Hauck, C., Böttcher, M., and Maurer, H.: A new model for estimating subsurface ice content based on combined electrical and seismic data sets, The Cryosphere, 5, 453–468, doi:10.5194/tc-5-453-2011, 2011.
Hausmann, H., Krainer, K., Brückl, E., and Mostler, W.: Internal structure and ice content of Reichenkar rock glacier (Stubai Alps, Austria) assessed by geophysical investigations, Permafrost Periglac., 18, 351–367, 2007.
Hilbich, C.: Time-lapse refraction seismic tomography for the detection of ground ice degradation, The Cryosphere, 4, 243–259, doi:10.5194/tc-4-243-2010, 2010.
Ikeda, A.: Combination of Conventional Geophysical Methods for Sounding the Composition of Rock Glaciers in the Swiss Alps, Permafrost Periglac., 17, 35–48, 2006.
IPCC: IPCC Fourth Assessment Report. Climate Change 2007 – The Physical Science Basis, Cambridge University Press, Cambridge, 2007.
Jaeger, C.: Rock mechanics and engineering, Cambridge University Press, Cambridge, 536 pp., 2009.
Johnston, J. E. and Christensen, N. I.: Seismic Anisotropy of Shales, J. Geophys. Res.-Earth, 100, 5991–6003, 1995.





TCD
6, 793–819, 2012



King, M. S.: Wave Velocities in Rocks as a Function of Changes in Overburden Pressure and Pore Fluid Saturants, Geophysics, 31, 50-73, 1966.
King, M. S.: Acoustic velocities and electrical properties of frozen sandstones and shales, Can. J. Earth Sci., 14, 1004–1013, 1977.
King, M. S.: The influence of clay-sized particles on seismic velocity for Canadian Arctic permafrost, Can. J. Earth Sci., 21, 19–24, 1984.
King, M. S., Zimmermann, R. W., and Corwin, R. F.: Seismic and electrical properties of unconsolidated permafrost, Geophys Prospec., 36, 349–364, doi:10.1111/j.1365-2478.1988.tb02168.x, 1988.
Kneisel, C., Hauck, C., Fortier, R., and Moorman, B.: Advances in geophysical methods for permafrost investigations, Permafrost Periglac., 19, 157–178, doi:10.1002/ppp.616, 2008.
Krautblatter, M.: Detection and quantification of permafrost change in alpine rock walls and implications for rock instability, Math.-Nat. Fakultät, Univerität Bonn, Bonn, 164 pp., 2009.
Krautblatter, M., Verleysdonk, S., Flores-Orozco, A., and Kemna, A.: Temperature-calibrated imaging of seasonal changes in permafrost rock walls by quantitative electrical resistivity tomography (Zugspitze, German/Austrian Alps), J. Geophys. Res.-Earth, 115, F02003, doi:10.1029/2008JF001209, 2010.
Krautblatter, M., Huggel, C., Deline, P., and Hasler, A.: Research perspectives for unstable high-alpine bedrock permafrost: measurement, modelling and process understanding, Permafrost Perigl. Process., doi:10.1002/ppp.740, in press., 2012.
Krus, M.: Feuchtetransport und Speicherkoeffizienten poröser mineralischer Baustoffe – theoretische Grundlagen und neue Meßtechniken, Fakultät für Bauingenieur- und Vermessungswesen, University of Stuttgart, Stuttgart, 1995.
Kurfurst, P. J. and Hunter, J. A.: Field and laboratory measurements of seismic properties of permafrost, Proceedings of a Symposium on Permafrost Geophysics, 1–15, 1977.
Leclaire, P., Cohen-Ténoudji, F., and Aguirre-Puente, J.: Extension of Biot's theory of wave propagation to frozen porous media, J. Acoust. Soc. Am., 96, 3753–3768, 1994.
Lo, T. W., Coyner, K. B., and Toksoz, M. N.: Experimental-Determination of Elastic-Anisotropy of Berea Sandstone, Chicopee Shale, and Chelmsford Granite, Geophysics, 51, 164–171, 1986.
Lock, G. S. H.: The growth and decay of ice, Studies in Polar Research, University Press, Cambridge, 2005.





TCD
6, 793–819, 2012



Matsuoka, N.: Mechanisms of Rock Breakdown by Frost Action – an Experimental Approach, Cold Reg. Sci. Technol., 17, 253–270, 1990.
Matsuoka, N., Hirakawa, K., Watanabe, T., Haeberli, W., and Keller, F.: The role of diurnal, annual and millenial freeze-thaw cycles in controlling alpine slope stability, 7th International Conference on Permafrost, Yellowknife, Canada, 711–717, 1998.
Matsuoka, N. and Murton, J.: Frost weathering: Recent advances and future directions, Permafrost Periglac., 19, 195–210, 2008.
McGinnis, L. D., Nakao, K., and Clark, C. C.: Geophysical identification of frozen and unfrozen ground, Antarctica, 2nd International Conference on Permafrost. Northamerican Contribution, Yakutsk, USSR, 136–146, 1973.
Murton, J. B., Peterson, R., and Ozouf, J. C.: Bedrock fracture by ice segregation in cold regions, Science, 314, 1127–1129, 2006.
Musil, M., Maurer, H., Green, A. G., Horstmeyer, H., Nitsche, F., Vonder Mühll, D., and Springman, S.: Shallow seismic surveying of an Alpine rock glacier, Geophysics, 67, 1701–1710, 2002.
Nakano, Y., Smith, M., and Martin, R. J.: Ultrasonic Velocities of Dilatational and Shear Waves in Frozen Soils, Water Resour. Res., 8, 1024–1030, 1972.
Nogués-Bravo, D., Araújo, M. B., Errea, M. P., and Martínez-Rica, J. P.: Exposure of global mountain systems to climate warming during the 21st Century, Global Environ. Chan., 17, 420–428, 2007.
NRC-Permafrost-Subcommitee: Glossary of Permafrost and related ground-ice terms, NRC Technical Memorandum, 142, 1–156, 1988.
Nur, A. and Simmons, G.: Effect of Saturation on Velocity in Low Porosity Rocks, Earth Planet. Sci. Lett., 7, 183–193, 1969.
Pandit, B. I. and King, M. S.: A study of the effects of pore-water salinity on some physical properties of sedimentary rocks at permafrost temperatures, Can. J. Earth Sci., 16, 1566–1580, 1979.
Pearson, C., Murphy, J., and Hermes, R.: Acoustic and Resistivity Measurements on Rock Samples Containing Tetrahydrofuran Hydrates - Laboratory Analogs to Natural-Gas Hydrate Deposits, J. Geophys. Res.-Solid, 91, 14132–14138, 1986.
Remy, J. M., Bellanger, M., and Homandetienne, F.: Laboratory Velocities and Attenuation of P-Waves in Limestones During Freeze-Thaw Cycles, Geophysics, 59, 245–251, 1994.





TCD
6, 793–819, 2012



Roethlisberger, H.: Seismic refraction soundings in permafrost near Thule, greenland, Proceedings of the first International Symposium on Arctic Geology, Calgary, Alberta, 970–980, 1961.
Sass, O.: Rock moisture measurements: Techniques, results, and implications for weathering, Earth Surf. Proc. Land., 30, 359–374, 2005.
Scott, W. J., Sellmann, P. V., and Hunter, J. A.: Geophysics in the study of permafrost, 3rd International Conference on Permafrost, Edmonton, Canada, 93–115, 1979.
Scott, W. J., Sellmann, P. V., and Hunter, J. A.: Geophysics in the study of permafrost, in: Geotechnical and Environmental Geophysics, edited by: Ward, S., Soc. of Expl. Geoph., Tulsa, 355–384, 1990.
Sondergeld, C. H. and Rai, C. S.: Velocity and resistivity changes during freeze-thaw cycles in Berea sandstone, Geophysics, 72, E99–E105, 2007.
Takeuchi, S. and Simmons, G.: Elasticity of Water-Saturated Rocks as a Function of Temperature and Pressure, J. Geophy. Res.-Earth., 78, 3310–3320, 1973.
Tharp, T. M.: Conditions for crack propagation by frost wedging, Geol. Soc. Am. Bull., 99, 94–102, 1987.
Thomsen, L.: Weak Elastic-Anisotropy, Geophysics, 51, 1954–1966, 1986.
Tice, A. R., Burrous, A. M., and Anderson, D. M.: Determination of unfrozen water in frozen soil by pulsed nuclear magnetic resonance, 3rd International Conference on Permafrost, Edmonton, Canada, 149–155, 1978.
Timur, A.: Velocity of compressional waves in porous media at permafrost temperatures, Geophysics, 33, 584–595, doi:10.1190/1.1439954, 1968.
Toksöz, M. N., Cheng, C. H., and Timur, A.: Velocities of Seismic-Waves in Porous Rocks, Geophysics, 41, 621–645, 1976.
Vernik, L. and Nur, A.: Ultrasonic Velocity and Anisotropy of Hydrocarbon Source Rocks, Geophysics, 57, 727–735, 1992.
Vlahou, I. and Worster, M. G.: Ice growth in a spherical cavity of a porous medium, J. Glaciol., 56, 271–277, 2010.
Walder, J. and Hallet, B.: A Theoretical-Model of the Fracture of Rock During Freezing, Geol. Soc. Am. Bull., 96, 336–346, 1985.
Walder, J. S. and Hallet, B.: The Physical Basis of Frost Weathering – toward a More Fundamental and Unified Perspective, Arctic Alpine Res., 18, 27–32, 1986.
Wang, Z. J.: Fundamentals of seismic rock physics, Geophysics, 66, 398–412, 2001.





TCD
6, 793–819, 2012



Wyllie, M. R. J., Gregory, A. R., and Gardner, L. W.: Elastic wave velocities in heterogeneous and porous media, Geophysics, 21, 41–70, 1956.
Wyllie, M. R. J., Gregory, A. R., and Gardner, L. W.: An experimental investigation of factors effecting elastic wave velocities in porous media, Geophysics, 23, 459–493, 1958.
Zimmerman, R. W. and King, M. S.: The effect of the extent of freezing on seismic velocities in unconsolidated permafrost, Geophysics, 51, 1285–1290, 1986.





TCD
6, 793–819, 2012



**Table 1.** Rock samples classified into lithological groups and physical properties. The table shows porosity ($\Phi$), degree of saturation ($S_r$) , p-wave velocity of a saturated ($V_{ps}$) and a frozen ($V_{pf}$) sample, p-wave velocity increase due to freezing ($\Delta V_p$), matrix velocity of a saturated ($V_{ms}$) and a frozen ($V_{mf}$) sample, matrix velocity increase due to freezing ($\Delta V_m$), anisotropy of a saturated ($A_s$) and a frozen sample ($A_f$) and the decrease of anisotropy due to freezing ($\Delta A$).

| Location (Country/Sample) | Lithology | Porosity | | P-wave velocity | | | | | | Matrix velocity | | | | | | Anisotropy | | |
|---|---|---|---|---|---|---|---|---|---|---|---|---|---|---|---|---|---|---|
| | | | | parallel | | | perpendicular | | | parallel | | | perpendicular | | | | | |
| | | $\Phi$ | $S_r$ | $V_{ps}$ | $V_{pf}$ | $\Delta V_p$ | $V_{ps}$ | $V_{pf}$ | $\Delta V_p$ | $V_{ms}$ | $V_{mf}$ | $\Delta V_m$ | $V_{ms}$ | $V_{mf}$ | $\Delta V_m$ | $A_s$ | $A_f$ | $\Delta A$ |
| | | [%] | | [ms$^{-1}$] | [ms$^{-1}$] | [%] | [ms$^{-1}$] | [ms$^{-1}$] | [%] | [ms$^{-1}$] | [ms$^{-1}$] | [%] | [ms$^{-1}$] | [ms$^{-1}$] | [%] | [%] | [%] | [%] |
| Steintälli/Matter Valley (CH/A5) | pyritic paragneiss | 1.04 ± 0.14 | 0.99 | 6261 | 6689 | 6.84 | 4774 | 5474 | 14.66 | 6479 | 6749 | 4.17 | 4869 | 5481 | 12.57 | 23.75 | 18.16 | 5.59 |
| Matterhorn/Matter Valley (CH/H1) | gneiss | 0.93 ± 0.12 | 1.00 | 5401 | 6099 | 12.92 | 4933 | 5399 | 9.45 | 5529 | 6148 | 11.20 | 5034 | 5432 | 7.91 | 8.67 | 11.48 | –2.81 |
| Zastler (D/X5) | gneiss | 0.95 ± 0.12 | 1.00 | 5699 | 5826 | 2.23 | 5007 | 5467 | 9.19 | 5858 | 5850 | –0.14 | 5110 | 5480 | 7.24 | 12.14 | 6.16 | 5.98 |
| *Gneiss* | *mean value* | *0.97 ± 0.04* | | | | *7.33 ± 3.73* | | | *11.10 ± 2.38* | | | *5.08 ± 4.08* | | | *9.24 ± 2.23* | | | *2.92* |
| Grossglockner (A/X2) | serpentine | 1.27 ± 0.16 | 1.00 | 5275 | 5873 | 11.34 | 4381 | 4672 | 6.64 | 5432 | 5923 | 9.04 | 4488 | 4687 | 4.43 | 16.95 | 20.45 | –3.50 |
| Matterhorn/Matter Valley (CH/H2) | amphibolite | 1.31 ± 0.08 | 0.96 | 4934 | 5929 | 20.17 | 4611 | 5356 | 16.16 | 5080 | 5992 | 17.95 | 4760 | 5401 | 13.47 | 6.55 | 9.66 | –3.12 |
| *Other metamorphic rocks* | *mean value* | *1.14 ± 0.13* | | | | *15.75 ± 4.41* | | | *11.40 ± 4.76* | | | *13.50 ± 4.46* | | | *8.95 ± 4.51* | | | *–3.31* |
| Steintälli/Matter Valley (CH/S1) | schisty quarz slate | 2.40 ± 0.12 | 0.96 | 5249 | 5805* | 10.59 | 1953 | 4373* | 123.91 | 5564 | 5906* | 6.15 | 1969 | 4400* | 123.46 | 62.79 | 24.67* | 38.12 |
| Steintälli/Matter Valley (CH/S4) | schisty quarz slate | 1.94 ± 0.10 | 0.94 | 5236 | 5942* | 13.48 | 1667 | 4425* | 165.45 | 5506 | 6037* | 9.64 | 1667 | 4455* | 167.25 | 68.16 | 25.53* | 42.63 |
| Steintälli/Matter Valley (CH/S3) | quarz slate | 1.49 ± 0.08 | 0.98 | 5116 | 6096 | 19.16 | 2615 | 3636 | 39.04 | 5294 | 6165 | 16.45 | 2655 | 3631 | 36.76 | 48.89 | 40.35 | 8.53 |
| Murtel (CH/X8) | greenschist | 1.86 ± 0.13 | 0.97 | 4682 | 5480 | 17.04 | 4504 | 5612 | 24.60 | 4869 | 5540 | 13.78 | 4683 | 5687 | 21.44 | 3.80 | 2.35 | 1.45 |
| Bliggspitze/Kauner Valley (A/A22) | mica schist | 1.56 ± 0.11 | 1.00 | 4329 | 5833 | 34.74 | 3882 | 5274 | 35.86 | 4454 | 5904 | 32.56 | 3942 | 5303 | 34.53 | 10.33 | 9.58 | 0.74 |
| Kitzsteinhorn (A/X13) | mica schist | 0.83 ± 0.06 | 0.91 | 5740 | 6224 | 8.43 | 5263 | 5786 | 9.94 | 5868 | 6270 | 6.85 | 5395 | 5799 | 7.49 | 8.31 | 7.04 | 1.27 |
| Muragl (CH/D2) | mica schist | 1.04 ± 0.07 | 1.00 | 5018 | 5373 | 7.07 | 4836 | 5355 | 10.73 | 5140 | 5408 | 5.21 | 4943 | 5352 | 8.27 | 3.63 | 0.34 | 3.29 |
| Corvatsch (CH/C1) | migmatic schist | 2.76 ± 0.27 | 0.94 | 4030 | 5293 | 31.34 | 2189 | 4356 | 98.99 | 4249 | 5385 | 26.74 | 2228 | 4395 | 97.26 | 45.68 | 17.70 | 27.98 |
| Corvatsch (CH/C2) | migmatic schist | 1.56 ± 0.15 | 0.99 | 5502 | 5978* | 8.65 | 1664 | 2595* | 55.95 | 5735 | 6051* | 5.51 | 1640 | 2579* | 57.26 | 69.76 | 56.59* | 13.17 |
| *Schists* | *mean value* | *1.48 ± 0.50* | | | | *16.72 ± 7.86* | | | *62.72 ± 44.49* | | | *13.65 ± 7.76* | | | *61.52 ± 45.18* | | | *15.24* |
| Aguille du Midi (F/M1) | granite | 1.31 ± 0.07 | 1.00 | 4228 | 5000 | 18.26 | 3583 | 4178 | 16.61 | 4332 | 5011 | 15.67 | 3663 | 4180 | 14.11 | 15.26 | 16.44 | –1.18 |
| Gemsstock (CH/X9) | granodiorite | 2.25 ± 0.05 | 0.99 | 5191 | 6078 | 17.09 | 4039 | 4759 | 17.83 | 5471 | 6194 | 13.22 | 4181 | 4808 | 15.00 | 22.19 | 21.70 | 0.49 |
| *Plutonic rocks* | *mean value* | *1.43 ± 0.55* | | | | *17.67 ± 0.59* | | | *17.22 ± 0.61* | | | *14.44 ± 1.24* | | | *14.56 ± 0.44* | | | *–0.35* |
| Präg (D/X6) | andesite | 3.03 ± 0.35 | 1.00 | 4345 | 6000 | 38.09 | 4935 | 5538 | 12.22 | 4618 | 6129 | 32.72 | 5286 | 5657 | 7.02 | 11.96 | 7.70 | 4.26 |
| Präg (D/X7) | andesite | 3.45 ± 0.40 | 1.00 | 4426 | 5541 | 25.19 | 4317 | 5248 | 21.57 | 4730 | 5678 | 20.04 | 4597 | 5360 | 16.60 | 2.46 | 5.29 | –2.83 |
| *Volcanic rocks* | *mean value* | *3.24 ± 0.21* | | | | *31.64 ± 6.45* | | | *16.89 ± 4.67* | | | *26.38 ± 6.33* | | | *11.81 ± 4.80* | | | *0.72* |
| Longyeardalen/Svalbard (N/L1) | Endalen Sandstone | 5.21 ± 0.96 | 1.00 | 3422 | 5130 | 49.91 | 5363 | 4904 | 37.64 | 3652 | 5290 | 44.85 | 3835 | 5031 | 31.19 | 3.96 | 4.41 | –0.45 |
| Longyeardalen/Svalbard (N/L2) | Endalen Sandstone | 6.03 ± 1.11 | 1.00 | 4521 | 5105 | 12.92 | 3989 | 4502 | 12.86 | 5139 | 5290 | 2.94 | 4440 | 4608 | 3.78 | 11.77 | 11.81 | –0.04 |
| *Clastic rocks* | *mean value* | *5.62 ± 0.41* | | | | *31.41 ± 18.50* | | | *25.25 ± 12.39* | | | *23.90 ± 20.96* | | | *17.49 ± 13.07* | | | *–0.25* |
| Zugspitze (D/A8) | Wetterstein Dolomite | 1.91 ± 0.16 | 1.00 | 3723 | 6383 | 71.45 | 1879 | 6068 | 222.94 | 3838 | 6500 | 69.36 | 1864 | 6161 | 230.53 | 49.53 | 4.93 | 44.59 |
| Saumur (F/K1) | Tuffeau Limestone | 45.16 ± 5.96 | 0.95 | 2247 | 4167 | 85.45 | 2014 | 4211 | 109.09 | 3566 | 5332 | 49.52 | 2647 | 5467 | 106.54 | 10.37 | 1.04 | 9.32 |
| *Carbonate rocks* | *mean value* | *23.54 ± 21.63* | | | | *78.45 ± 7.00* | | | *166.01 ± 56.93* | | | *59.44 ± 9.93* | | | *168.53 ± 62.00* | | | *26.96* |

* indicates lowest sample temperatures above –10 °C.





TCD
6, 793–819, 2012



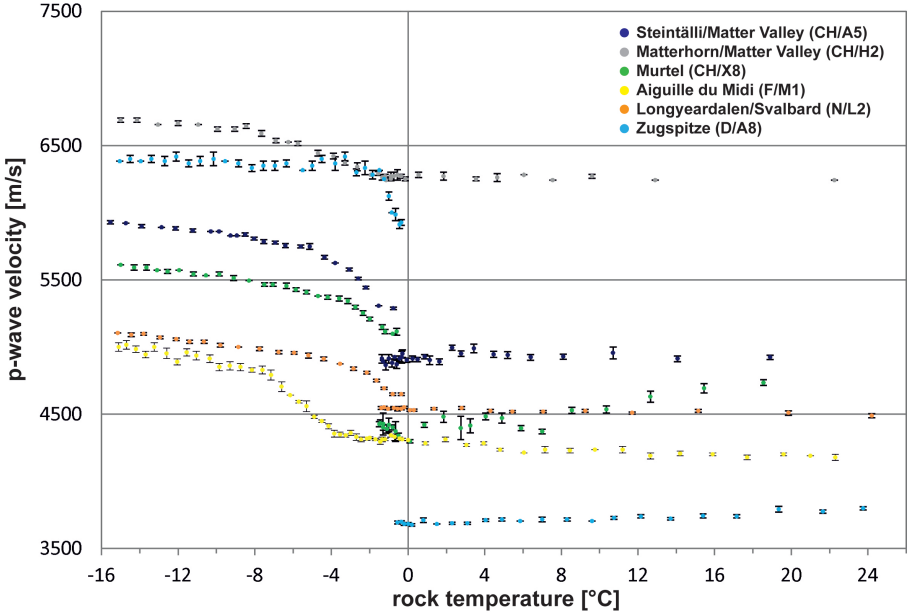


**Fig. 1.** P-wave velocity of igneous, metamorphic and sedimentary rock samples measured parallel to cleavage or bedding plotted against rock temperature; error bars indicate mean deviation.





TCD
6, 793–819, 2012



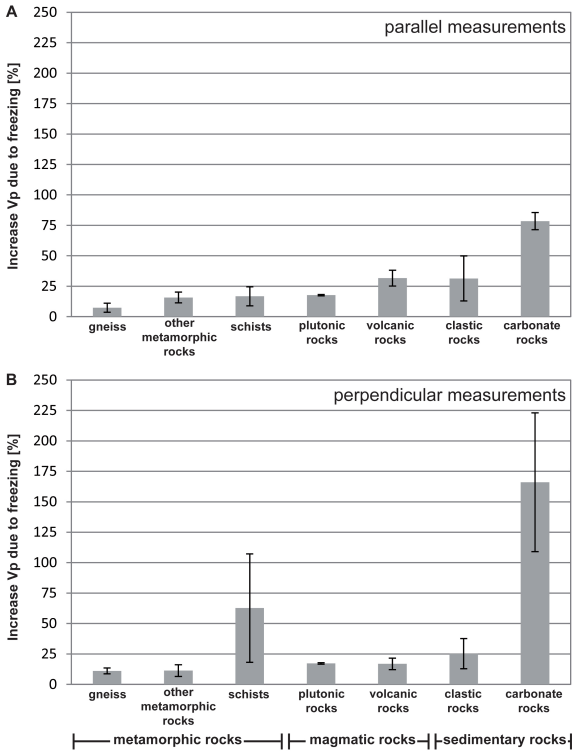


**Fig. 2.** P-wave velocity increase in percent for rock groups classified based on lithology; **(A)** parallel to cleavage/bedding and **(B)** perpendicular to cleavage/bedding; error bars indicate mean deviation.





TCD
6, 793–819, 2012



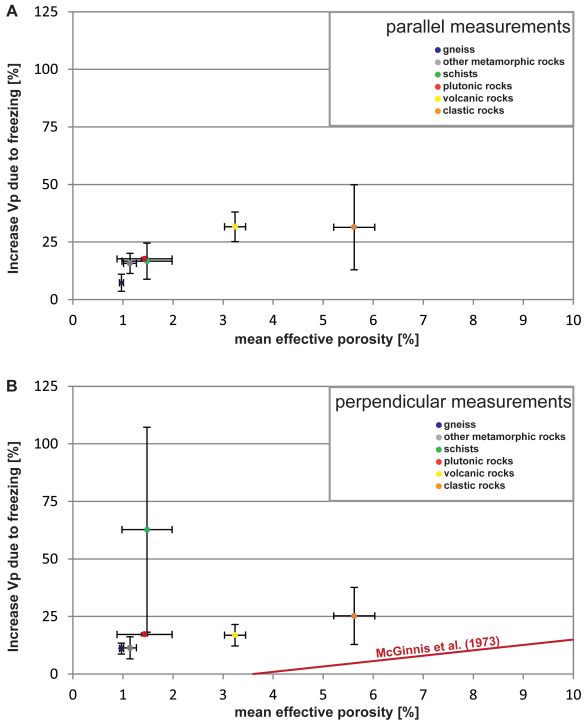


**Fig. 3.** Percentage p-wave velocity increase due to freezing plotted against mean effective porosities for six different rock groups; **(A)** parallel to cleavage or bedding, **(B)** perpendicular to cleavage/bedding, the red line indicates the linear regression based on McGinnis et al. (1973); error bars indicate the mean deviation. This shows that McGinnis et al. (1973) is incapable of explaining p-wave velocity increase in hard low-porosity rocks.





TCD
6, 793–819, 2012



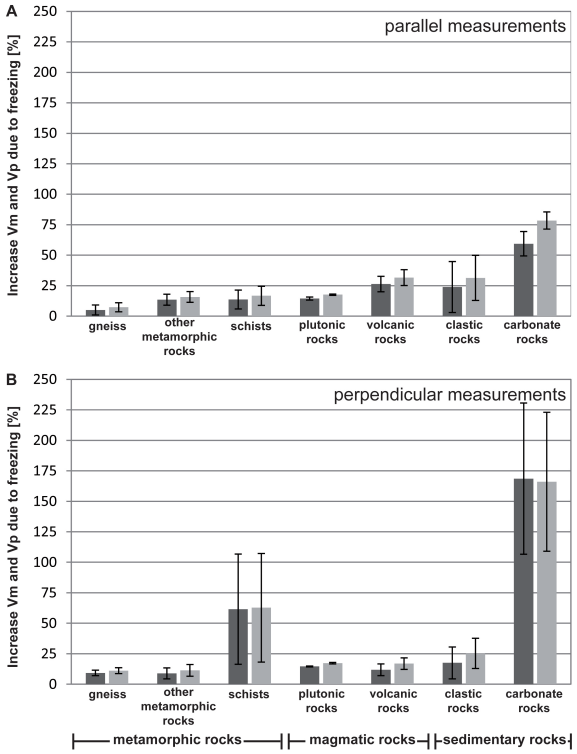


**Fig. 4.** Increase of matrix velocity (dark grey columns) and p-wave velocity (grey columns) for different rock groups, **(A)** measured in parallel direction to cleavage/bedding, **(B)** measured perpendicular to cleavage/bedding; error bars indicate mean deviation.





TCD
6, 793–819, 2012